# Prestin is the motor protein of cochlear outer hair cells

**Jing Zheng*, Weixing Shen*, David Z. Z. He*, Kevin B. Long†, Laird D. Madison† & Peter Dallos***

** Auditory Physiology Laboratory (The Hugh Knowles Center), Departments of Neurobiology and Physiology and Communciation Sciences and Disorders, Northwestern University, Evanston, Illinois 60208, USA*
*† Center for Endocrinology, Metabolism, and Molecular Medicine, Department of Medicine, Northwestern University Medical School, Chicago, Illinois 60611, USA*

**The outer and inner hair cells of the mammalian cochlea perform different functions. In response to changes in membrane potential, the cylindrical outer hair cell rapidly alters its length and stiffness. These mechanical changes, driven by putative molecular motors, are assumed to produce amplification of vibrations in the cochlea that are transduced by inner hair cells. Here we have identified an abundant complementary DNA from a gene, designated *Prestin*, which is specifically expressed in outer hair cells. Regions of the encoded protein show moderate sequence similarity to pendrin and related sulphate/anion transport proteins. Voltage-induced shape changes can be elicited in cultured human kidney cells that express prestin. The mechanical response of outer hair cells to voltage change is accompanied by a 'gating current', which is manifested as nonlinear capacitance. We also demonstrate this nonlinear capacitance in transfected kidney cells. We conclude that prestin is the motor protein of the cochlear outer hair cell.**

Cochlear hair cells are non-neuronal epithelial cells that transduce acoustic signals. Outer hair cells (OHCs) are responsible for the exquisite sensitivity and frequency-resolving capacity of the normal mammalian hearing organ[1]; they provide local mechanical amplification (the 'cochlear amplifier') in the form of feedback. In contrast, inner hair cells convey auditory information to the brain. Outer hair cells have cylindrical somata of constant diameter and variable length. When their membrane potential is altered[2–5], somatic shape changes of up to 5% occur; the cell shortens when depolarized and lengthens when hyperpolarized[3,5]. Length changes do not depend on either ATP or $Ca^{2+}$ (ref. 6), and they can be elicited with unchanging amplitude at microsecond rates up to high audio frequencies[7,8]. Motile responses are accompanied by charge movement, which is reflected in nonlinear capacitance[9,10], akin to the translocation of gating charges of voltage-gated ion channels[11]. This nonlinear capacitance is widely used as a 'signature' of the electromotile process[10,12]. Motility is also accompanied by a change in the axial stiffness of the cell[13]. By virtually any test, electromotility and electrically-induced stiffness changes are correlated (D.Z.Z. and P.D., unpublished data) and we collectively describe them as

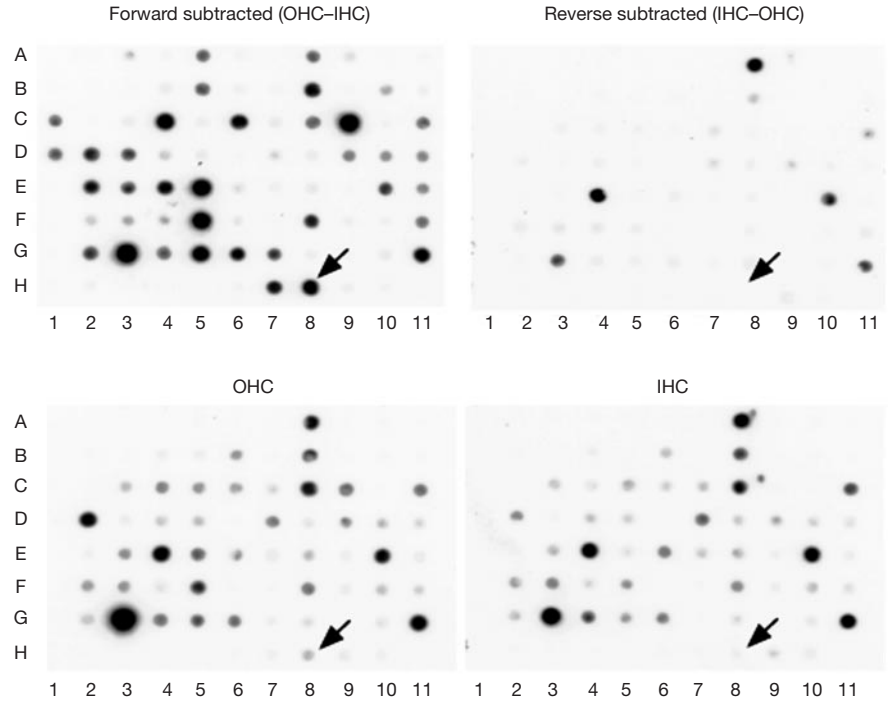


**Figure 1** *Pres* fragment identification. Four identical cDNA blots of PCR-amplified inserts derived from the subtracted cDNA library were separately hybridized with radioactive forward-subtracted probe (OHC–IHC), reverse-subtracted probe (IHC–OHC), and OHC and IHC cDNA probes. Note, for example, that the samples at the H8 locations (arrows) show strong signals in OHC and OHC–IHC hybridization blots and little or no signal in the IHC and IHC–OHC blots. Samples such as these were selected for sequencing.

voltage-dependent mechanical changes of the OHC, hereafter called 'electromechanics'. These observations make it apparent that the fast mechanical changes in OHCs are powered by a molecular motor that is fundamentally different from other biological force generators, such as the myosin, kinesin or dynein families. The OHC molecular motor performs direct, rapid, reversible electro-mechanical conversion.

Outer hair cell electromotility is the probable result of the concerted action of a large number of independent molecular motors that are closely associated with the cell's basolateral membrane[6,14,15], possibly by the densely packed 10-nm particles[16] seen therein. A general hypothesis is that the particles are the molecular sensor motors and here we attempt to identify them. There have been some suggestions as to the identity of these motor molecules. On the basis of similarities between the cortical structures of erythrocytes and OHCs, the motor molecule has been proposed to be a modified anion exchanger[17,18]. Because their shallow voltage dependence matches that of charge movement in OHCs, transporters have been favoured, as opposed to modified voltage-dependent channels, as likely candidates[12]. One suggestion has been that the motor is related to a fructose transporter, GLUT5 (ref. 19). Until now, molecular identification of the motor protein has not been achieved. In as much as the most distinguishing feature of this molecular motor is its speed, we designate it as prestin, from the musical notation presto. The gene (*Prestin*) coding for this protein is abbreviated *Pres*.

## Cloning of *Pres* and the properties of prestin

Our molecular approach to identify the OHC sensor–motor protein faced two initial challenges: first, isolation of complementary DNA from limited amounts of biological material; and second, recognition of the candidate motor protein cDNA among the isolated unknown genes. Isolation of a sufficient number of OHCs is a fairly routine task. Obtaining comparable numbers of inner hair cells (IHCs), however, required some modification of techniques (D.Z.Z.H. *et al.*, unpublished data). We were able to isolate messenger RNA from about 1,000 OHCs and 1,000 IHCs and used mRNA reverse transcription followed by 5′-mRNA cap and oligo dT-dependent PCR amplification to obtain OHC and IHC cDNA pools.

Our strategy for recognizing the cDNAs that might encode the candidate motor protein was based on the following assumptions: the protein is expressed in OHCs and not in the non-motile IHC; ontogenic expression should relate to the known development of electromechanical responses[20]; the protein should be relatively abundant in OHCs; the protein should be a transmembrane protein; and electromechanical responses should be demonstrable when the protein is expressed in a heterologous system. We expected that gene expression related to mechano-electric transduction and genomic, metabolic and structural functions would be shared by these two types of hair cell; therefore, we applied a suppression subtractive hybridization polymerase chain reaction (PCR) procedure to amplify and enrich the OHC cDNA pool for uniquely expressed gene products[21]. This procedure uses two rounds of cDNA hybridization to subtract out common OHC cDNAs using a vast excess of IHC cDNA. The unique fragments are amplified by PCR, digested with *Rsa*I and cloned to create a library of candidate clones. This technique is useful because it simultaneously enriches differentially expressed cDNA fragments and suppresses non-target DNA amplification.

About 1,300 fragment clones were screened with four cDNA pools (OHC–IHC, IHC–OHC, OHC unsubtracted and IHC unsubtracted) to identify differentially expressing clones (Fig. 1). Once false positives were excluded, 487 clones were identified as differentially expressing, and of these 108 were sequenced. Because of duplicates, these 108 sequences identified 50 unique cDNA fragments. Eighteen of the clones had sequences highly similar to known proteins, whereas 32 were thought to be unique in that there were no obvious homologous sequences in the genetic database. Eleven of the 32 clones had apparent open reading frames and were examined in greater detail by dot-blot hybridization with radioactively labelled cloned cDNA against immobilized OHC and IHC cDNA pools. *Pres* was one of the 11 candidate clones whose differential expression was most consistent with our assumptions about the motor protein. *Pres* fragments in the PCR subtracted library were abundant (>10% of 487 differentially expressed clones) and showed consistent differential hybridization with OHC- and IHC-derived probes (Fig. 1). Using one of these *Pres* cDNA *Rsa*I fragments as a probe, we subsequently isolated three cDNA clones from a λgt11 gerbil adult cochlea library (provided by B. Schulte). The largest of these clones was 4.1 kilobase (kb) with an open reading frame of 2,232 base pairs (bp), encoding a 744-amino-acid protein (Fig. 2). The sequence around the putative translation start site contains a consensus Kozak sequence[22] and an in-frame

```
gPrestin   1 ....MDHAEENEIPVATQKYHVERPIFSHPVLQERLHVKDKVSESIGDKLKQAFTCTPKKIRNIIYMFLPITKWLPAYKFKEYVLGDLVSGISTGVLQLP
rPendrin   1 MAARDRRSEPPQLAEYSCSYAVSRPVYSELAFQQQRERRLPERRTLRDSLARSCSCSRKRAFGALKALLPILDWLPKYRVKEWLLSDIISGVSTGLVGTL

          97 QGLAFAMLAAVPPVFGLYSSFYPVIMYCFFGTSRHISIGPFAVISLMIGGVAVRLVPDD.IVIPGG....VNATN.GTEARDALRVKVAMSVTLLSGIIQ
         101 QGMAYALLAAVPVQYGLYSAFFPILTYFVFGTSRHISVGPFPVVSLMVGSVVLSMAPDDHFLVPSGNGSTLNTTTLDTGTRDAARVLLASTLTLLVGIIQ

         191 FCLGVCRFGFVAIYLTEPLVRGFTTAAAVHVFTSMLKYLFGVKTKRYSGIFSVVYSTVAVLQNVKNLNVCSLGVGLMVFGLLLGGKEFNERFKEKLPAPI
         201 LVFGGLQIGFIVRYLADPLVGGFTTAAAFQVLVSQLKIVLNVSTKNYNGVLSIIYTLIEIFQNIGDTNIADFIAGLLTIIVCMAVKELNDRFKHKIPVPI

         291 PLEFFAVVMGTGISAGFNLHESYSVDVVGTLPLGLLPPANPDTSLFHLVYVDAIAIAIVGFSVTISMAKTLANKHGYQVDGNQELIALGICNSIGSLFQT
         301 PIEVIVTIIATAISYGANLEANYNAGIVKSIPSGFLPPVLPSVGLFSDMLAASFSIAVVAYAIAVSVGKVYATKHDYIIIDGNQEFIAFGISNVFSGFFSC

         391 FSISCSLSRSLVQEGTGGKTQLAGCLASLMILLVILATGFLFESLPQAVLSAIVIVNLKGMFMQFSDLPFFWRTSKIELTIWLTTFVSSLFLGLDYGLIT
         401 FVATTALSRTAVQESTGGKTQVAGLISAVIVMVAIVALGKLLEPLQKSVLAAVVIANLKGMFMQVCDVPRLWKQNKTDAVIWVFTCIMSIILGLDLGLLA

         491 AVIIALLTVIYRTQSPSYKVLGQLPDTDVYIDIDAYEEVKEIPGIKIFQINAPIYYANSDLYSNALKRKTGVNPALIMGARRKAMRKYAKEVGNANIANA
         501 GLLFGLLTVVLRVQFPSWNGLGSVPSTDIYKSITHYKNLEEPEGVKILRFSSPIFYGNVDGFKKCVKSTVGFDAIRVYNKRLKALRRIQKLIKKGQLRAT

         591 AVVKVDGEVDGENATKPE...EEDDEVKYP..PIVIKTTFPEELL..QRFMPQTENVHTIILDFTQVNFIDSVGVKTLAVMVKEYGDVGIYVYLAGCSPQV
         601 KNGIISDVGSSNNAFEPDEDVEEPEELDIPTKEIEIQVDWNSELPVKVNVPKVP.IHSLVLDCGAVSFLDVVGVRSLRMIVKEFQRIDVNVYFALLQDDV

         684 VNDLTRNRFFENPALKELLFHSIHDAVLGSHVREAMAEQEASAPPPQDDMEPNATPTTPEA 744
         700 LEKMEQCGFFDDNIRKDRFFLTVHDAIL.......YLQNQAKSREGQDSLLETITLIQDCKDPLELMEAEINEEELDVQDEAMRRLAS 780
```

**Figure 2** Amino-acid sequence of gerbil prestin and its homology to rat pendrin. Identical prestin/pendrin residues are shown in red, and highly similar amino acids are in green. Prestin residues, which are in bold and underlined, indicate the 12 differences for the deduced human sequence derived from exons 1–6 of the known *PRES* genomic sequence (first 295 residues). The position of the signature sulphate transport motif is boxed (black). A blue box indicates the positive charge cluster and a yellow box denotes the negative-charge cluster. GenBank accession numbers: gerbil prestin, AF230376; rat pendrin, AF167412.

stop codon is present 12 bases upstream of this predicted start site. There is a short 223-bp untranslated 5′ end and a large 1,654-bp, 3′ untranslated region. A computer search with the *Pres* sequence revealed that about one-third of the human *PRES* gene had been sequenced as part of the human chromosome 7 effort (BAC clone RG107G13, bases 99,895 to >113,558). The amino-acid homology between human and gerbil prestin, deduced from the genomic sequence of the first 6 exons, is 98% (Fig. 2).

Analysis of the prestin sequence revealed that its highest homology was to members of a family of sulphate/anion transport proteins including pendrin and DRA (down-regulated in adenoma)[23,24]. The pendrin homology (40%) was of particular interest because this chloride–iodide transport protein is a cause of the genetically inherited deafness observed in Pendred's syndrome[25]. This homology, although modest overall, is similar to the homology among other members of the sulphate/anion transport family. Because we were using gerbil cDNA, and only rat, mouse and human pendrin sequences were known at the time, it was necessary to prove that prestin was not the gerbil homologue of pendrin; first it should be noted that mouse pendrin is expressed in the endolymphatic duct and sac, the utricle and saccule and in the external sulcus but not in the organ of Corti[26] in the cochlea; second, we cloned an 824-bp fragment of gerbil pendrin cDNA, the sequence of which was distinct from that of prestin (data not shown). The gerbil pendrin amino-acid sequence derived from the above cDNA fragment was 88% homologous to that of human pendrin, but only 38% homologous to that of gerbil prestin.

The protein prestin (744 amino acids; relative molecular mass ($M_r$) 81.4 K) is hydrophobic, with ~50% non-polar residues; 27.8% of the protein is composed of the amino acids valine, leucine and isoleucine. Computer modelling of the amino-acid sequence produces ambiguous results using multiple modelling programs. Specifically, the models TMHMM[27] and TMPred[28] report ambiguous results as to the number and location of transmembrane regions and are unable to predict the topology of the amino and carboxy termini in relation to the membrane. In comparison, when pendrin is subjected to the same modelling programs, 11 transmembrane regions and an intracellular N terminus are unambiguously predicted. A complete topology analysis using antibodies directed against prestin epitopes, affinity labelling and mutagenesis will probably be required to clarify the nature of the protein/membrane interface. Two distinctive charged regions are located in the C-terminal region. A positive-charge cluster is located at residues 557–580; adjacent to this is a negative-charge cluster at residues 596–613 (Fig. 2). Prestin's overall predicted hydropathy profile is similar to those of pendrin, DRA and other members of the sulphate/anion transport family. The homology to pendrin is highest in the 50-amino-acid region (97–146) that encompasses the sulphate transport motif (109–130), but does not have long regions of identity elsewhere. Instead, there is a pattern of moderate homology by both amino-acid identity and similarity throughout the protein with multiple, discrete, 8–12-residue segments of identity. The charged cluster regions of prestin and pendrin are conserved in their net charges, but are otherwise not remarkably homologous. The proteins differ most in the region between the two charge clusters and at the termini. Prestin shows high homology in the sulphate transport region, a highly conserved domain found in homologues in organisms as distant as yeast, *Caenorhabditis elegans* and plants. However, both human and gerbil prestin differ from the consensus sequence at three positions (Fig. 3)[29]. Consequently, although prestin appears to be related to sulphate transporters, these differences in the conserved region suggest that the protein may have distinct properties.

We then determined the tissue-specific and developmental expression pattern of *Pres* in the gerbil. Northern analysis with a *Pres* probe did not detect expression in liver, lung, brain, spleen, ovary, kidney, muscle or heart (total RNA 20 μg; data not shown). Virtual northern dot-blot analysis using cDNA prepared from IHC, OHC, mature and newborn organs of Corti, and thyroid revealed expression only in mature OHCs and 20-day-old organs of Corti (Fig. 4a). Similar results were obtained using *Pres*-specific primers and a qualitative PCR assay (Fig. 4b). Both virtual northern and PCR showed progressively increasing *Pres* expression in isolated organ of Corti from birth up to 20 days after birth (Fig. 4c, d), by which time electromotility is fully developed in the altricial gerbil[20]. In OHCs, the motors are generally thought to be congruent with abundant ~10-nm membrane particles[16,30]. The density of these particles in gerbil OHCs shows a developmental increase, decelerating towards adult values 16–18 days after birth[31]. Thus, the ontogenic expression of *Pres* is similar to

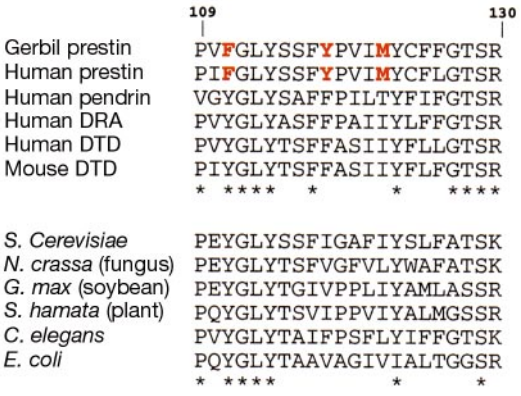


**Figure 3** Comparison of sulphate transport motifs. The amino-acid sequence of gerbil and human prestin is compared with the same domain in other members of the sulphate/anion transport family. Top panel, alignment of prestin, pendrin, DRA and DTD (diastrophic dysplasia) from human and rodent species. Bottom panel, sulphate transport motifs from a variety of putative transporters in lower organisms. Amino-acid residue numbers refer to the sequence of gerbil prestin. Invariant residues are indicated by the asterisks below the sequence panels. Similarly divergent residues in the two prestin sequences are coloured red. The sulphate transport motif is defined by PROSITE PS01130.

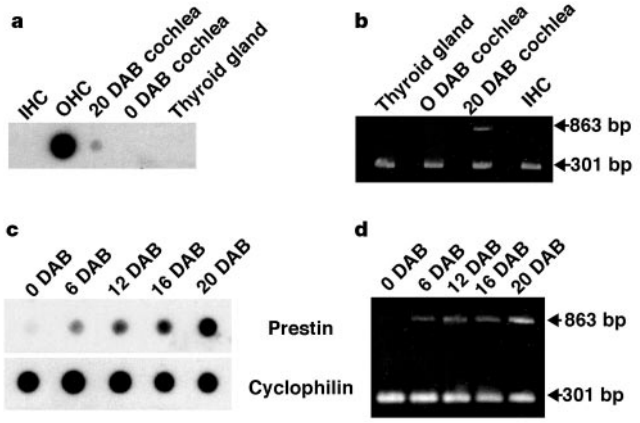


**Figure 4** Analysis of *Pres* expression in SMART cDNA from different tissues and at different developmental ages. **a**, Virtual northern dot-blot analysis. cDNA pools derived from mRNA of gerbil tissues were hybridized with a $^{32}$P-labelled *Pres* probe. **b**, PCR analysis. cDNA pools synthesized from different tissues were amplified with *Pres* and cyclophilin-specific primers. In **a** and **b**, 'cochlea' refers to organ of Corti-derived tissue. **c**, Virtual northern dot-blot analysis. cDNA pools derived from organ of Corti mRNA at 0, 6, 12, 16 and 20 DAB were hybridized with a $^{32}$P-labelled *Pres*-specific probe. The blot was then stripped and rehybridized with a $^{32}$P-labelled cyclophilin probe. **d**, PCR analysis. cDNA pools derived from organ of Corti mRNA at 0, 6, 12, 16 and 20 DAB were amplified with *Pres* and cyclophilin-specific primers. DAB, days after birth. The exposure time was shorter in **a** than in **c** because of the strong signal from OHC cDNA.

that of membrane particles, electromotility and the onset of high sensitivity hearing.

### Functional tests of prestin

To investigate the function of the prestin cDNA, we sought to examine the functional properties of prestin in eukaryotic cells. To accomplish this, we subcloned *Pres* into the eukaryotic expression vector pcDNA3.1. We also created a C-terminal epitope-tagged (V5) version (pcDNA6/V5-HisA vector) to determine expression of the full-length protein in transfected cells. The expression of the V5 version was examined by indirect immunofluorescence to assure its presence in transfected cells, as we did not have an antibody directed against prestin. The epitope-modified prestin was apparently located in the cell membrane, with a punctate distribution in permeabilized cells (data not shown). In addition, western blot analysis using an anti-V5 antibody against transfected cell extracts showed production of the appropriate sized protein (data not shown).

To test the sensor–motor function of prestin, voltage-dependent charge movement was measured from TSA201 cells after transient transfection of unmodified, native *Pres* cDNA. A second plasmid (pEGFP-N2) containing the green fluorescent protein (GFP) cDNA was used as an independent marker for successful transfection of the cells. Transfection efficiency was 30–40% as judged from the fluorescence of GFP in transfected cells. Consistent with this, under voltage clamp, 36.8% of cells transfected with *Pres* alone displayed transient capacitive currents, using a standard subtraction protocol after blocking ionic currents (Fig. 5a). In experiments conducted on cells cotransfected with prestin and GFP cDNA, transient capacitive currents were obtained from 91.8% of the GFP-positive cells (45 out of 49). In contrast, untransfected cells ($n = 20$) or cells transfected with only the control plasmid ($n = 28$) had no measurable nonlinear capacitance. The capacitive currents were directed towards the outside as the membrane potential was depolarized and towards the inside as it was hyperpolarized. Charges transferred at command onset and offset were roughly equal. The decay of transient currents was rapid (100–200 μs) and could be well fitted to a single exponential. The voltage protocol used to estimate membrane capacitance and charge transfer across the membrane was an ascending stair-step voltage waveform[15] (Fig. 5b). The membrane capacitance was fitted to the derivative of a first-order Boltzmann equation (ref. 15; see Methods and Fig. 5c). In a group of seven cells, these curve fits yielded values of $Q_{max} = 1.76 \pm 0.20$ pC, $V_{1/2} = 57.30 \pm 2.98$ nV, $1/\alpha = kT/ze = 28.00 \pm 2.13$ mV and $C_{lin} = 20.50 \pm 2.65$ pF, respectively (mean ± s.e.m.). The valence can be calculated from $\alpha$, $z = 0.91$ (refs 10, 12, 32). The average charge density, a possible measure of transiently transfected motor protein density in TSA201 cells, was 5,360 $\mu m^{-2}$. The numerical values that characterize the charge movement ($V_{1/2}$, $z$) are quite similar to those obtained for OHCs[15]. The maximum charge and charge density are less in the transfected cells, even though the linear capacitance is about the same as that of an average OHC.

In OHCs, nonlinear capacitive current and electromotility can be reversibly blocked by sodium salicylate[33–35]. As further evidence that transient currents stem from the transfected motor protein, salicylate was locally applied to cells that had been shown to present charge movement. Sodium salicylate (10 mM) reduced the transient currents to 15.5 ± 2.9% of control ($n = 8$, Fig. 5d). Of these, three cells showed recovery after 2–5 min of washing (to 88.4 ± 8.8% of control value). Finally, the existence of nonlinear capacitance was tested in 15 cells that were transfected with both GFP and human pendrin cDNA. None of the GFP-positive cells showed nonlinear capacitance. This result is significant because of the similarity of pendrin and prestin, indicating the specificity of our candidate motor protein. It also indicates that the electrophysiological results are not simply the consequence of the introduction of an anion transport protein.

Of the two manifestations of motor function—nonlinear capacitance and motility—the former is much easier to measure. Although electromotility has been shown in patches isolated from OHC basolateral membrane[36], the cell's cortical cytoskeleton facilitates the conversion of mechanical molecular events to gross cellular deformation[6,37,38]. In TSA201 cells, the organized cytoskeletal network is probably missing. Consequently, even if the motor protein is expressed, gross cellular deformation is expected to be very small. Furthermore, OHCs are efficient producers of axial motility because of their cylindrical shape. Fast mechanical effects occur at constant cell volume and are generally assumed to be the result of a change in cell-surface area, owing to the aggregate conformational shape changes of large numbers of motor proteins[6,14]. A spherical cell cannot change its surface area while its volume remains constant, whereas a cylindrical cell can[38]. So that the generally spherical TSA201 cells might produce measurable motility, we distorted them to alter their shape by drawing them into a suction pipette (microchamber[39]), thereby producing a dumbbell or hourglass shape (Fig. 6a). In spite of these difficulties, and our inability to test for GFP co-transfection (our motility measurement setup lacks fluorescence capability), we succeeded in demonstrating electromotility in 7 out of 31 cells tested. Two of the best responses are shown in Fig. 6b, along with a trace from a non-transfected, non-responsive cell. Our usual electrical driving signal was a brief 200-Hz sinusoid. Sodium salicylate produces a reversible decrease in the electromotile response (Fig. 6c), just as it does in OHCs[33–35]. To examine motility at higher frequencies, comparisons between responses at 200 and 1,000 Hz are shown in Fig. 6d and e. When corrected for the characteristics of the recording system, the two responses are essentially identical (Fig. 6e), consistent with OHC data obtained in the past[7].

### Implications

We have used a logical strategy to isolate the cDNA that is responsible for the unique electromechanical function of OHCs,

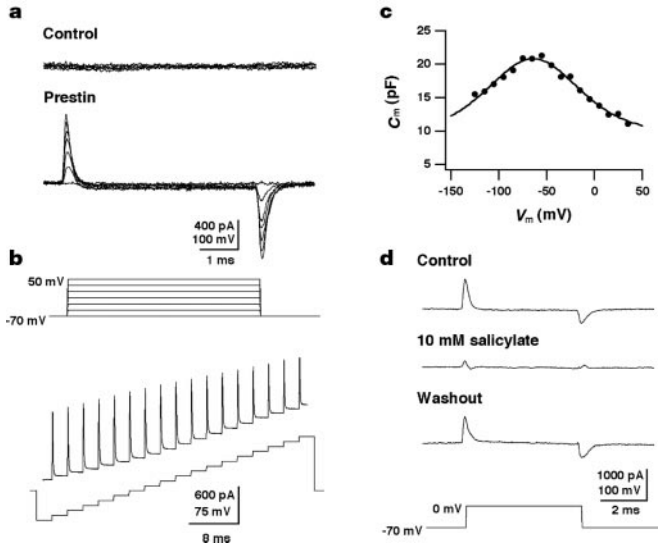


**Figure 5** Voltage-dependent charge movement in TSA201 cells. Recordings were made 24–60 h after transfection. **a**, Charge movement measured as transient capacitive currents using a standard subtraction technique (P/4). The cell was held at −70 mV; voltage steps are 20 mV to +50 mV. **b**, Stair-step protocol quantifies the voltage dependence of nonlinear capacitance. Voltage was stepped from −130 to +40 mV in 10 mV increments of 2.5 ms each. Twenty presentations were averaged. **c**, The membrane capacitance-voltage curve was obtained from the stair-step current trace in panel **b**. Data points were fitted with the derivative of a Boltzmann function (equation (1)). **d**, Localized application of 10 mM sodium salicylate reversibly blocked the charge movement.

and have shown that prestin conveys mechanical responsiveness to a heterologous system, which is almost indistinguishable from that measured in OHCs.

The fact that a portion of the human *PRES* gene has been sequenced and mapped allows us to predict the location of the motor protein in relation to the other members of its family and to consider any relationship to genetic loci known to be related to hearing disorders or deafness. The bacterial artificial chromosome clone (RG107G13) which contains a portion of the *PRES* gene at its 3′ end has a single known other gene, *RELN*, which is about 50 kb centromeric to the *PRES* gene fragment. This location is ~3.7 Mb centromeric to the location of the *PENDRIN (PDS)* and *DRA* genes. Thus, it appears likely that *PRES* is located in an as yet unsequenced portion of 7q31, centromeric to *PDS* and *DRA* and 50 kb telomeric to the *RELN* gene. At present there are two autosomal recessive loci (DFNB) mapped to 7q31 in addition to the *PDS* gene: DFNB14 (ref. 40) and DFNB17 (ref. 41). DFNB14 is the most likely candidate to be *PRES*, because it maps at a centromeric position to the *PDS* gene locus, whereas DFNB17 maps to the telomeric side of *PDS* and *DRA*. The proof that DFNB14 is itself distinct from *PDS* is derived from the fact that the *PDS* exons were sequenced and appeared to be normal, indicating that the causative mutation was distinct from that seen in Pendred's syndrome[40]. The clinical phenotype in this kindred is a congenital, sensorineural, autosomal recessive form of non-syndromic deafness, which is consistent with our prediction of prestin's functional role.

Our results support earlier work on OHCs, which showed that neither the subsurface cortical lattice nor the subsurface cisterns is essential for electromotility[36–38]. It is unlikely that either of these organelles would be present in TSA201 cells, in either their native or transfected form. Our demonstration of nonlinear capacitance and motility simplifies the concept of electromechanical changes in OHCs and obviates the need for exotic schemes. Presumed conformational changes of prestin, resulting in a change of cell-surface area, produce dimensional changes in the cell. This is the basic electromotile response[2–5]. It is yet to be determined whether stiffness changes accompany these shape changes in TSA201 cells, as they do in OHCs, thus expressing the full electromechanical process.

The reliance of the mammalian cochlea on local, OHC-based amplification is widely accepted, but there is no universal agreement

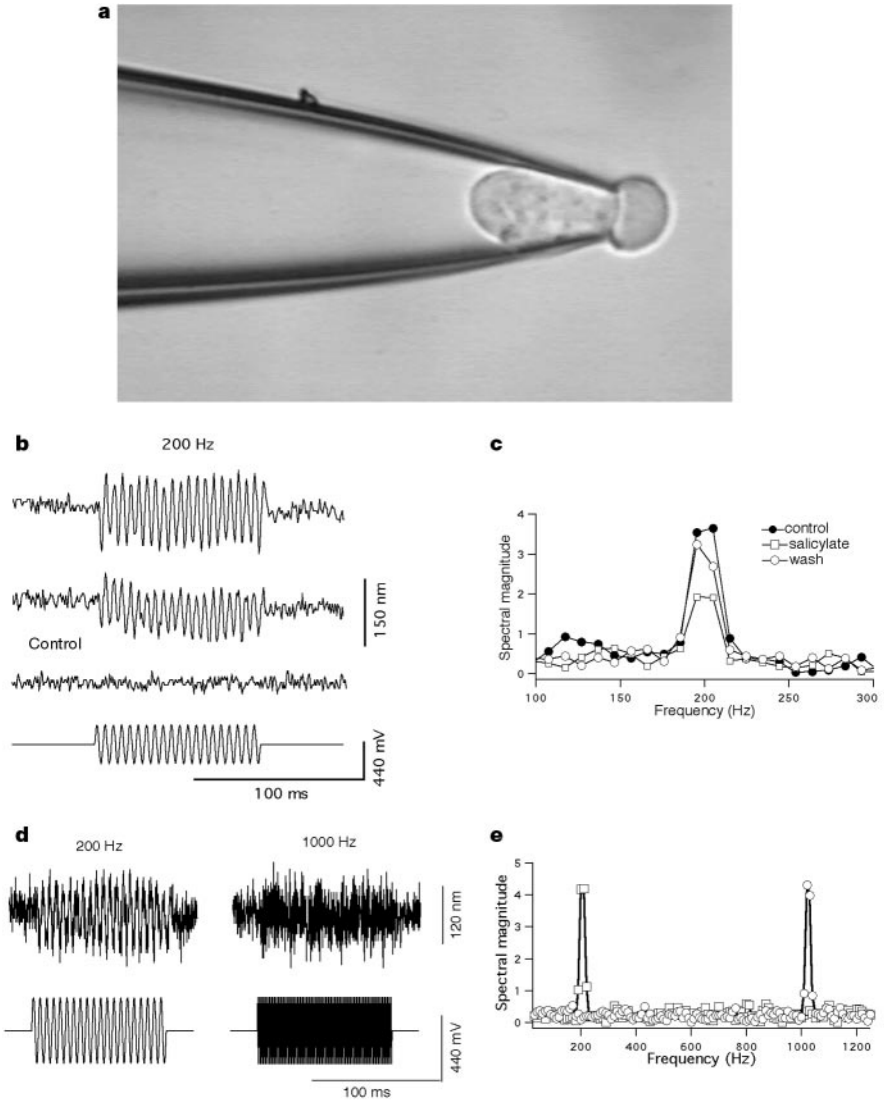


**Figure 6** Examples of voltage-dependent motility expressed in TSA201 cells. **a**, Video image of a TSA201 cell partially drawn into a microchamber. Motility was measured at the farthest excluded membrane segment. **b**, Top two traces, motile responses from two transfected cells. Third trace, lack of motile response from cell transfected with control plasmid only. Fourth trace, stimulus waveform. **c**, Effect of 10 mM sodium salicylate in the external bathing solution on the response, shown by Fourier transforms of the responses. **d**, Response (top) and stimulus (bottom) waveforms with two different command frequencies. **e**, Fourier transforms of the two response segments in **d**, including 1.2-dB correction for the system's frequency response. Response waveforms are the averages of 200 presentations. **c** and **e** are plotted with arbitrary ordinates.

about the amplifying mechanism. One view is that, powered by the cell's receptor potential, OHC electromotility provides mechanical feedback and thereby amplification[1,12]. This view places the motor process in the cell's basolateral membrane and calls for a motor protein to drive somatic shape changes. An alternative concept is that amplifcation arises as a byproduct of the cell's forward transducer process and thus resides in the stereocilia[42]. Whichever mechanism dominates, the existence of electromechanical action in OHCs is indisputable. We have now identified the gene that codes for a specialized motor protein that produces this electromechanical action when expressed in cells that in their native form do not show this phenomenon.

Isolated OHCs are capable of producing an average maximum axial isometric (stall) force of ~6 nN (D.Z.Z.H. and P.D., unpublished data and ref. 43). From the number of molecules producing this force it can be estimated that the individual molecular stall force is on the order of 2.4 pN. In comparison, the stall force of kinesin is 5–6 pN (ref. 44). We note the potential of prestin to perform as a fast, voltage-driven actuator, individually or in assemblies, forming the basis of futuristic nanomachinery. □

## Methods

### Tissue preparation and *Pres* cDNA isolation by subtractive PCR hybridization

Animal care and use procedures were approved by the Northwestern University Institutional Review Board. Mature gerbils were killed and the organ of Corti and associated basilar membrane were isolated as described[45]. After brief trypsin treatment and triturаton, OHCs and IHCs were isolated in a low-calcium solution. Using a glass pipette, the cells were separated depending on their morphological appearance and were collected in LiCl buffer. mRNA was isolated from tissue using 20 μl oligo-dT magnetic beads (Dynal). cDNA pools were created with Superscript II RNAase $H^-$ reverse transcriptase (Gibco) followed by amplification with a 5′ cap and oligo dT-dependent PCR technique according to manufacturer's specifications (SMART PCR, Clontech). These cDNA pools were used for PCR subtractive hybridization, qualitative PCR and virtual northern (cDNA) dot-blot hybridization experiments. The PCR subtractive hybridization procedures, control reactions and subcloning were according to the manufacturer's instructions (PCR Select cDNA Subtraction Kit, Clontech).

Clones were subjected to a differential screening procedure using a PCR-Select Differential Screening Kit (Clontech). PCR-amplified cDNA inserts from these clones were denatured and vacuum filtered onto four identical nylon membranes. Each cDNA sample was separately hybridized with one of the following probes: forward subtracted (OHC–IHC) cDNA; reverse subtracted (IHC–OHC) cDNA; unsubtracted OHC cDNA; and unsubtracted IHC cDNA. These cDNA pools were random primed labelled with [$^{32}$]dCTP and hybridized to the blots. Positively hybridizing clones were scored for differential hybridization with forward (OHC–IHC) and reverse (IHC–OHC) subtracted probes. This differential expression was confirmed by correlation with simultaneous differential hybridization with the original unsubtracted OHC and IHC cDNA pools. Sequencing was carried out using dRhodamine terminator cycle sequencing (ABI Prism) and an automated DNA sequencer (Model 377, Perkin Elmer). DNA and amino-acid sequences were compared and analysed using sequence analysis software of GCG and TMHMM[27] and TMpred[28].

### Virtual northern (cDNA) dot-blot hybridization

SMART cDNA (0.5 μg) from gerbil thyroid, IHC, OHC, and 0-, 6-, 12-, 16- and 20-day-old organs of Corti was denatured and vacuum filtered onto membranes. A *Pres* cDNA fragment (1,067-bp *Nco*I restriction fragment) was radioactively labelled with [$^{32}$P]dATP and used as a probe (Strip-EZ Kit and UltraHyb buffer, Ambion).

### PCR

PCR reactions used templates of 200 ng of SMART cDNA from gerbil thyroid, newborn and adult organ of Corti, isolated IHC and organ of Corti from various postnatal ages (0 to 20 DAB). *Pres*-specific primers (sense; 5′-TACCTCACGGAGCCGCTGGT-3′; antisense; 5′-GCAGTAATCAGTCCGTAGTCC-3′) were used to amplify an 863-bp fragment from the cDNA. Cyclophilin primers (sense; 5′-TGGCACAGGAGGAAAGAGCATC-3′; antisense; 5′-AAAGGGCTTCTCCACCTCGATC-3′) that amplify a 301-bp DNA fragment were used as internal control. Cycle parameters were 3 min at 94 °C followed by 25–30 cycles of 94 °C for 45 s, 56 °C for 45 s and 72 °C for 1 min, with a final extension at 72 °C for 10 min.

### Transient transfection

TSA201 cells, clones of human embryonic kidney 293 cells that express the simian virus 40 large T-antigen[46] in a stable manner, were cultured in D-MEM with 5% fetal calf serum, 100 U of penicillin per ml and 100 μg of streptomycin per ml. Cells were plated for 24 h before calcium phosphate transfection[47]. The transfection reaction mixture contained: (1) control plasmid, pcDNA3.1; (2) 2 μg of *Pres* cDNA plasmid; (3) 2 μg *Pres* cDNA plasmid plus 0.2 μg of GFP plasmid as transfection marker; or (4) 2 μg pendrin cDNA plasmid plus 0.2 μg GFP plasmid.

### Functional verification

After 24 h the transfected cells were used for electrophysiological and physical measurements. Large, rounded, non-clustered TSA201 cells, exhibiting considerable granulation, were selected for electrophysiological and motility experiments.

### Capacitance measurements

Whole-cell voltage-clamp recordings were made with an Axopatch 200B amplifier (Axon Instruments). Recording pipettes had open tip resistances of 2–3 MΩ and were filled with internal solution containing (in mM): 140 CsCl, 2 $MgCl_2$, 10 EGTA, 10 HEPES; pH 7.2. The external solution contained (in mM): 120 NaCl, 20 TEA-Cl, 2 $CoCl_2$, 2 $MgCl_2$, 10 HEPES, 5 glucose; pH 7.2. Osmolarity was adjusted to 300 mosm $l^{-1}$ with glucose. Capacitive currents were filtered at 5 kHz and digitized at 50 kHz using pClamp 7.0 software (Axon Instruments). Voltage-dependent capacitance was measured using two methods. First, a standard P/4 linear subtraction procedure[11] was used to detect the presence of nonlinear charge movement. Second, after nonlinear transient current was detected, a stair-step voltage protocol was used to obtain the parameters of charge movement[15]. For each voltage step, the measured membrane capacitance ($C_m$) was plotted as a function of membrane voltage ($V_m$) and fitted with the derivative of a Boltzmann function:

$$C_m = \frac{Q_{max}\alpha}{\exp[\alpha(V_m - V_{1/2})](1+\exp[-\alpha(V_m - V_{1/2})])^2} + C_{lin} \quad (1)$$

where $Q_{max}$ is maximum charge transfer, $V_{1/2}$ is the voltage at which the maximum charge is equally distributed across the membrane, $C_{lin}$ is linear capacitance and $\alpha = ze/kT$ is the slope factor of the voltage dependence of charge transfer where $k$ is Boltzmann's constant, $T$ is absolute temperature, $z$ is valence and $e$ is electron charge. From the stair-step analysis, we have obtained the membrane resistance $R_m = 130.45 \pm 20.14$ MΩ ($n = 7$).

### Motility measurements

TSA201 cells were drawn into a microchamber[39] with gentle suction (Fig. 6a). The microchamber was mounted on a 3D micromanipulator attached to the stage of a Zeiss inverted microscope. The most distal part of the excluded segment of the cell was imaged onto a photodiode with a rectangular slit interposed into the light path. A change of photocurrent signified cell extension or contraction. The signal was current-to-voltage transformed, amplified, A/D converted and averaged ($n = 200$). The command voltage, delivered between the electrolyte solutions (L15, Gibco) surrounding and filling the microchamber, produces different voltage drops on the included and excluded cell-membrane segments, determined by the electrical voltage-divider effect of these membranes[14]. The voltage-divider ratio is not known; consequently we do not report actual driving voltages in the motility experiments. During motility measurements, the location of the cell within the slit was monitored by a video camera placed behind the slit. The appearance of the whole cell in the microchamber was also continuously displayed with the aid of a second video camera. This permitted independent verification of a lack of movement of the microchamber itself.

Received 6 December 1999; accepted 28 March 2000.


1. Dallos, P. in *The Cochlea* (eds Dallos, P., Popper, A. N. & Fay, R. R.) 1–43 (Springer, New York, 1996).
2. Brownell, W. E., Bader, C. R., Bertrand, D. & de Ribaupierre, Y. Evoked mechanical responses of isolated outer hair cells. *Science* **227,** 194–196 (1985).
3. Ashmore, J. F. A fast motile response in guinea-pig outer hair cells: the cellular basis of the cochlear amplifier. *J. Physiol. (Lond.)* **388,** 323–347 (1987).
4. Santos-Sacchi, J. & Dilger, J. P. Whole cell currents and mechanical responses of isolated outer hair cells. *Hearing Res.* **35,** 143–150 (1988).
5. Kachar, B., Brownell, W. E., Altschuler, R. A. & Fex, J. Electrokinetic shape changes of cochlear outer hair cells. *Nature* **322,** 365–368 (1986).
6. Holley, M. C. & Ashmore, J. F. On the mechanisms of a high frequency force generator in outer hair cells isolated from the guinea pig cochlea. *Proc. R. Soc. Lond. Ser. B* **232,** 413–429 (1988).
7. Dallos, P. & Evans, B. N. High frequency motility of outer hair cells and the cochlear amplifier. *Science* **267,** 2006–2009 (1995).
8. Frank, G., Hemmert, W. & Gummer, A. W. Limiting dynamics of high-frequency electromechanical transduction of outer hair cells. *Proc. Natl Acad. Sci. USA* **96,** 4420–4425 (1999).
9. Ashmore, J. F. in *Mechanics of Hearing* (eds Kemp, D. & Wilson, J. P.) 107–113 (Plenum, New York, 1999).
10. Santos-Sacchi, J. Reversible inhibition of voltage-dependent outer hair cell motility and capacitance. *J. Neurosci.* **11,** 3096–3110 (1991).
11. Armstrong, C. M. & Bezanilla, F. Charge movement associated with the opening and closing of the activation gates of the Na channels. *J. Gen. Physiol.* **63,** 533–552 (1974).
12. Ashmore, J. F. in *Sensory Transduction* (eds Corey, D. P. & Roper, S. D.) 395–412 (Rockefeller Univ. Press, New York, 1992).
13. He, D. Z. Z. & Dallos, P. Somatic stiffness of cochlear outer hair cells is voltage dependent. *Proc. Natl Acad. Sci. USA* **96,** 8223–8228 (1999).
14. Dallos, P., Evans, B. N. & Hallworth, R. On the nature of the motor element in cochlear outer hair cells. *Nature* **350,** 155–157 (1991).
15. Huang, G. & Santos-Sacchi, J. Mapping the distribution of the outer hair cell motility voltage sensor by electrical amputation. *Biophys. J.* **65,** 2228–2236 (1993).
16. Forge, A. Structural features of the lateral walls in mammalian cochlear outer hair cells. *Cell Tissue Res.* **265,** 473–483 (1991).

17. Kalinec, F. & Kachar, B. Inhibition of outer hair cell electromotility by sulfhydryl specific reagents. *Neurosci. Lett.* **157,** 231–234 (1993).
18. Knipper, M. *et al.* Immunological identification of candidate proteins involved in regulating shape changes of outer hair cells. *Hearing Res.* **86,** 100–1100 (1995).
19. Géléoc, G. S. G., Casalotti, S. O., Forge, A. & Ashmore, J. F. A sugar transporter as a candidate for the outer hair cell motor. *Nature Neurosci.* **2,** 713–719 (1999).
20. He, D. Z. Z., Evans, B. N. & Dallos, P. First appearance and development of electromotility in neonatal gerbil outer hair cells. *Hearing Res.* **78,** 77–90 (1994).
21. Diatchanko, L. *et al.* Suppression subtractive hybridization: a method for generating differentially regulated or tissue-specific cDNA probes and libraries. *Proc. Natl Acad. Sci. USA* **93,** 6025–6030 (1996).
22. Kozak, M. An analysis of 5′ noncoding sequences from 699 vertebrate messenger RNAs. *Nucleic Acids Res.* **15,** 8125–8148 (1987).
23. Everett, L. A. *et al.* Pendred syndrome is caused by mutations in a putative sulphate transporter gene (PDS). *Nature Genet.* **17,** 411–422 (1997).
24. Moseley, R. H. *et al.* Downregulated in adenoma gene encodes a chloride transporter defective in congenital chloride diarrhea. *Am. J. Physiol.* **276,** 185–192 (1999).
25. Scott, D. A., Wang, R., Kreman, T. M., Sheffield, V. C. & Karniski, L. P. The Pendred syndrome gene encodes a chloride–iodide transport protein. *Nature Genet.* **4,** 440–443 (1999).
26. Everett, L. A. & Green, E. D. A family of mammalian anion transporters and their involvement in human genetic diseases. *Hum. Mol. Genet.* **8,** 1883–1891 (1999).
27. Sonnhammer, E. L. L., Heijne, G. von & Krogh, A. A hidden Markov model for predicting transmembrane helices in protein sequences. *Proc. 6th Int. conf. Intelligent Syst. Mol. Biol. (ISMB98)* (eds Glasgow, J. *et al.*) 175–182 (Amer. Assoc. for Artificial Intelligence Press, Menlo Park, CA, 1998).
28. Hofman, K. & Stoffel, W. Tmbase—a database of membrane spanning protein segments. *Biol. Chem.* **374,** 166 (1993).
29. Sandal, N. N. & Marcker, K. A. Similarities between a soybean nodulin, Neurospora crassa sulphate permease II and a putative human tumour suppressor. *Trends Biochem. Sci.* **19,** 19 (1994).
30. Holley, M. C., Kalinec, F. & Kachar, B. Structure of the cortical cytoskeleton in mammalian outer hair cells. *J. Cell. Sci.* **102,** 569–580 (1992).
31. Souter, M., Nevill, G. & Forge, A. Postnatal development of membrane specialisations of gerbil outer hair cells. *Hearing Res.* **91,** 43–62 (1995).
32. Iwasa, K. H. Effect of stress on the membrane capacitance of the auditory outer hair cell. *Biophys. J.* **65,** 492–498 (1993).
33. Shehata, W., Brownell, W. E. & Dieler, R. Effects of salicylate on shape, electromotility and membrane characteristics of isolated hair cells from the guinea pig cochlea. *Acta Oto-Laryngol. (Stockholm)* **111,** 707–718 (1991).
34. Kakehata, S. & Santos-Sacchi, J. Effects of salicylate and lanthanides on outer hair cell motility and associated gating charge. *J. Neurosci.* **16,** 4881–4889 (1996).
35. Tunstall, M. J., Gale, L. E. & Ashmore, J. F. Action of salicylate on membrane capacitance of outer hair cells from the guinea-pig cochlea. *J. Physiol. (London)* **485,** 739–752 (1995).
36. Kalinec, F., Holley, M. C., Iwasa, K., Lim, D. J. & Kachar, B. A membrane-based force generation mechanism in auditory sensory cells. *Proc. Natl Acad. Sci. USA* **89,** 8671–8675 (1992).
37. Huang, G. J. & Santos-Sacchi, J. Motility voltage sensor of the outer hair cell resides within the lateral plasma membrane. *Proc. Natl Acad. Sci. USA* **91,** 12268–12272 (1994).
38. Adachi, M. & Iwasa, K. H. Electrically driven motor in the outer hair cell: effect of a mechanical constraint. *Proc. Natl Acad. Sci. USA* **96,** 7244–7249 (1999).
39. Evans, B. N., Dallos, P. & Hallworth, R. in *Cochlear Mechanisms* (eds Wilson, J. P. & Kemp, D. T.) 205–206 (Plenum, London, 1989).
40. Mustapha, M. *et al.* Identification of a locus on chromosome 7q31, DFNB14, responsible for prelingual sensorineural non-syndromic deafness. *Eur. J. Hum. Genet.* **6,** 548–551 (1998).
41. Greinwald, J. H. Jr *et al.* Localization of a novel gene for nonsyndromic hearing loss (DFNB17) to chromosome region 7q31. *Am. J. Med. Genet.* **78,** 107–113 (1998).
42. Hudspeth, A. J. Mechanical amplification of stimuli by hair cells. *Curr. Opin. Neurobiol.* **7,** 480–486 (1997).
43. Iwasa, K. H. & Adachi, M. Force generation in the outer hair cell of the cochlea. *Biophys. J.* **73,** 546–555 (1997).
44. Svoboda, K. & Block, S. M. Force and velocity measured for single kinesin molecules. *Cell* **77,** 773–784 (1994).
45. He, D. Z. Z. Relationship between the development of outer hair cell electromotility and efferent innervation: a study in cultured organ of Corti of neonatal gerbils. *J. Neurosci.* **15,** 3634–3643 (1997).
46. Margolskee, R. F., McHendry-Rinde, B. & Horn, R. Panning transfected cells for electrophysiological studies. *Biotechniques* **15,** 906–911 (1993).
47. Graham, F. L. & van der Eb, A. J. Transformation of rat cells by DNA of human adenovirus 5. *Virology* **54,** 536–539 (1973).

## Acknowledgements

We thank L. H. Pinto and J. S. Takahashi for their comments on the manuscript. We also thank P. Kopp for providing the human pendrin cDNA, B. Schulte for providing the λgt11 gerbil cochlea library, and Y. Tang, M. Brenner and J. Cheng for technical assistance. This work was primarily supported by a Senior Fellowship from the McKnight Endowment Fund for Neuroscience to P.D. and the National Institute on Deafness and other Communication Disorders, NIH.

Correspondence and requests for materials should be addressed to P.D. (e-mail: p-dallos@nwu.edu). *Pres* has been deposited in the GenBank under accession number AF230376.